

Dalton Transactions

Accepted Manuscript



This is an *Accepted Manuscript*, which has been through the Royal Society of Chemistry peer review process and has been accepted for publication.

Accepted Manuscripts are published online shortly after acceptance, before technical editing, formatting and proof reading. Using this free service, authors can make their results available to the community, in citable form, before we publish the edited article. We will replace this *Accepted Manuscript* with the edited and formatted *Advance Article* as soon as it is available.

You can find more information about *Accepted Manuscripts* in the [Information for Authors](#).

Please note that technical editing may introduce minor changes to the text and/or graphics, which may alter content. The journal's standard [Terms & Conditions](#) and the [Ethical guidelines](#) still apply. In no event shall the Royal Society of Chemistry be held responsible for any errors or omissions in this *Accepted Manuscript* or any consequences arising from the use of any information it contains.

Blue-Emitting Heteroleptic Ir(III) Phosphors with Functional 2,3'-Bipyridine or 2-(Pyrimidin-5-yl)pyridine Cyclometalates

Tainan Duan,^a Ting-Kuang Chang,^a Yun Chi,^{a,*} Jin-Yun Wang,^b Zhong-Ning Chen,^{b,*} Wen-Yi Hung,^{c,*} Chang-Hsuan Chen,^c Gene-Hsiang Lee,^d

^a Department of Chemistry, National Tsing Hua University, Hsinchu 30013, Taiwan;

E-mail: ychi@mx.nthu.edu.tw

^b Fujian Institute of Research on the Structure of Matter, CAS, State Key Laboratory of Structural Chemistry, China; E-mail: czn@fjirsm.ac.cn

^c Institute of Optoelectronic Sciences, National Taiwan Ocean University, Keelung 202, Taiwan; E-mail: wenhung@mail.ntou.edu.tw

^d Instrumentation Center, National Taiwan University, Taipei 10617, Taiwan

Abstract

We have synthesized four Ir(III) metal complexes (**1** – **4**) bearing dual fluorine-free cyclometalates that derived from 2',6'-dimethoxy-4-*t*-butyl-2,3'-bipyridine (pypy)H or 2-(2,4-dimethoxypyrimidin-5-yl)-4-*t*-butylpyridine (pmpy)H and a third ancillary, e.g. 5-pyridin-2-yl-pyrazolate (Pz) or 5-pyridin-2-yl-pyrrolide (Pr), respectively. The Ir(III) complexes **3** and **4** were examined by X-ray diffraction studies for providing the structural proofs. Photophysical properties were next measured in CH₂Cl₂ at RT, among which the pypy complexes **1** and **2** showed an identical structured emission with E₀₋₀ peak located at 458 nm, while the corresponding pmpy derivative **3** displayed the most blue-shifted E₀₋₀ peak at 444 nm. Organic light-emitting diodes (OLEDs) were fabricated using multiple layered architecture and aforementioned phosphor at 8 wt.% doping level. The associated OLED performances, cf. max. E.Q.E. = 9.0 %, 14.3 %, 5.8 % and 9.4 % and CIE_{x,y} coordinates at (0.16, 0.22), (0.16, 0.24), (0.16, 0.17) and (0.16, 0.20) at 100 cd/m² for phosphors **1** – **4** in sequence,

confirmed their potential as blue dopant for phosphorescent OLEDs.

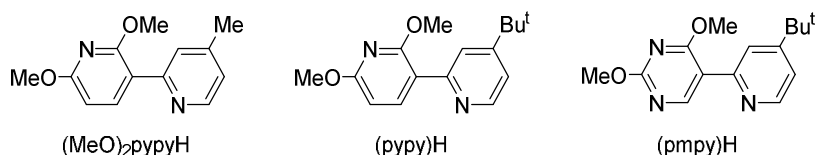
Introduction

Organic light emitting diodes (OLEDs) hold great promise for the emerging commercial market of both the flat panel displays and solid state luminaries. For continuous improving relevant technologies, it is essential to acquire various light emitting materials, particularly the transition-metal based phosphors with higher efficiencies and having all three elementary colors, namely: red, green and blue. Unlike the green and red-emitting phosphors, for which many OLED devices with excellent performances have been reported, the development of blue-emitting phosphors still remains as a challenging task, simply because it demanded a higher lying emitting excited states.¹⁻⁴ Hence, the higher emission energy lowers the gap between emitting excited state and metal-centered *dd* excited state, and allows fast population to this long-lived, non-emissive excited state.⁵ The consequence is to induce a rapid decline in efficiency upon blue-shifting the emission color (or reducing the gap between these states).^{6, 7} Method for avoiding this behaviour is to utilize chelates with higher ligand-field strength, i.e. those can form stronger metal-ligand bonding and destabilize the metal-centered *dd* excited state.

Prototypical examples of blue-emitting Ir(III) phosphors include these with chromophores derived from nitrogen-donors such as pyridinyl azole,⁸⁻¹¹ and from cyclometalating heteroaromatics such as 2,4-difluorophenylpyridine and relevances,^{12, 13} (2,4-difluoro-3-trifluoromethylphenyl)pyridine and derivatives,^{14, 15} (2,4-difluoro-3-trifluoromethylketone-phenyl)pyridine and analogues,¹⁶ (2,4-difluoro-3-perfluorobutanone-phenyl)-4-methylpyridine,¹⁷ (2,4-difluoro-3-cyanophenyl)pyridine,¹⁸ phosphoryl and sulfonyl-substituted 2,4-difluorophenylpyridine,^{19, 20} diaryl-1,3,4-oxadiazole,²¹ 1-aryl-1,2-pyrazole,^{22, 23} 2',6'-difluoro-2,3'-bipyridine,²⁴ 2',6'-dialkoxy-2,3'-bipyridine,^{25, 26} 5-aryl-1,2,4-triazole,²⁷ and 4-aryl-1,2,3-triazole,²⁸ as well as NHC carbene such as

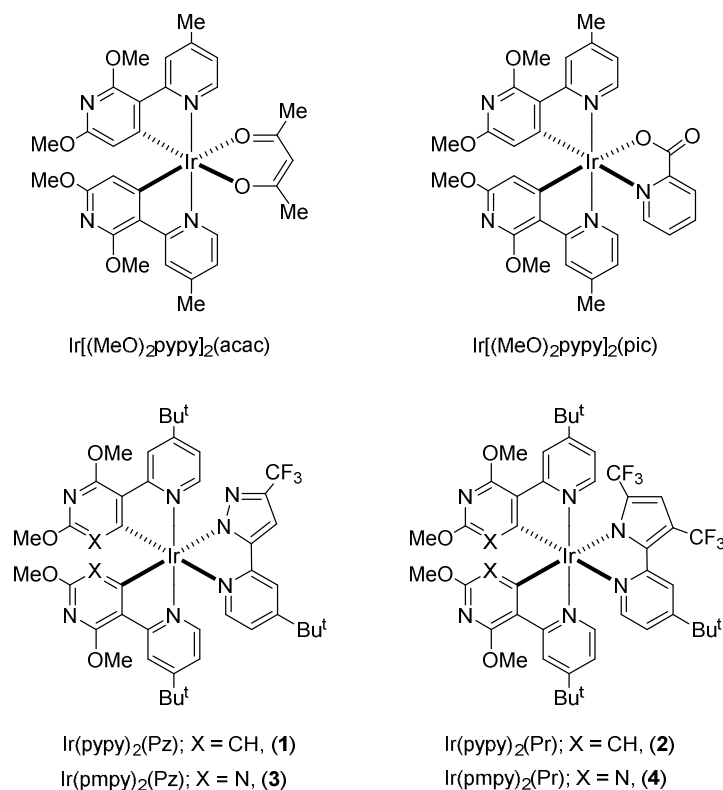
1-phenyl-3-methylimidazole,²⁹ 1-benzyl-3-methylimidazole,³⁰ and N-dibenzofuranyl-N'-methylimidazole.³¹ Their common design is the introduction of electron rich (or deficient) substituents on the cyclometalating chromophores that is in control of the LUMO (or HOMO), respectively.

In this article, we report the synthesis and testing of four blue-emitting Ir(III) phosphors, which consist of either the cyclometalating 2,3'-bipyridine (ppy)H or 2-(pyrimidin-5-yl)-pyridine (pmpy)H, and a third ancillary deriving from substituted 5-pyridin-2-yl-pyrazolate or pyrrolide. Both (ppy)H and (pmpy)H chelates are selected as they belong to a class of fluorine-free aromatics, and phosphors without these chelates are expected to have greater chemical stability and longer lifespan for the as-fabricated OLED devices.^{32, 33}



The Ir(III) phosphors with 2',6'-dimethoxy-4-methyl-2,3'-bipyridine chelates have been documented, namely: Ir[(MeO)₂ppy]₂(acac) and Ir[(MeO)₂ppy]₂(pic), acac = acetylacetonate and pic = picolate, for which the OLED with Ir[(MeO)₂ppy]₂(pic) gave an optimized external quantum efficiency (EQE) of 15.3% and CIE_{x,y} coordinate of (0.16, 0.28) at 100 cd/m².³⁴ With an aim of further improving the efficiency and color hue, we repeated the reactions using similar 2',6'-dimethoxy-4-*t*-butyl-2,3'-bipyridine chelate, denoted as (ppy)H, and with more electron deficient ancillaries, i.e. 2-[3-(trifluoromethyl)-1*H*-pyrazol-5-yl]-4-*t*-butylpyridine (Pz)H³⁵ and 2-[3,5-bis(trifluoromethyl)-1*H*-pyrrol-2-yl]-4-*t*-butylpyridine (Pr)H,³⁶ with the goal of acquiring more efficient blue-emitting phosphors, cf. Ir(ppy)₂(Pz) (**1**) and Ir(ppy)₂(Pr) (**2**). Relevant syntheses using 2-(2,4-dimethoxypyrimidin-5-yl)-4-*t*-butylpyridine chelate, i.e. (pmpy)H were also attempted, for which the isolated Ir(pmpy)₂(Pz) (**3**)

and Ir(pmpy)₂(Pr) (**4**) have exhibited the bluer emission, due to the greater $\pi\pi^*$ gap of pmpy cyclometalates. The associated details are given in the results and discussion section.



Experimental section

General Information and Materials. All reactions were performed under a nitrogen atmosphere and solvents were distilled from appropriate drying agents prior to use. Commercially available reagents were used without further purification unless otherwise stated. ¹H and ¹⁹F NMR spectra were measured with a Varian Mercury-400 in CDCl₃. UV-Vis spectra were recorded on a HITACHI U-3900 spectrophotometer. Detail of measurement of steady-state emission in both solution and solid state was described in our previous reports.³⁷ Lifetime studies were measured with Edinburgh FL 900 photon-counting system. Electrochemical behaviors were investigated by using cyclic voltammetry (CV) on a CHI621A Electrochemical

Analyzer. The elemental analysis was carried out on a Heraeus CHN-O Rapid Elementary Analyzer. Mass spectra were recorded on a JEOL SX-102A instrument operating in Electron Impact (EI) or Fast Atom Bombardment (FAB) mode.

Preparation of 4-*t*-butyl-2',6'-dimethoxy-2,3'-bipyridine (pypy)H and 2-(2,4-dimethoxypyrimidin-5-yl)-4-*t*-butylpyridine (pmpy)H. A mixture of 4-*t*-butyl-2-chloropyridine (1.0 equiv.), 2,6-dimethoxypyridine-3-boronic acid (or 2,4-dimethoxypyrimidine-5-boronic acid, 1.1 equiv.), Pd(dppf)Cl₂ (0.05 equiv.) and K₂CO₃ (5 equiv.) in toluene and water (v:v, 5:1) was heated at 100 °C for 24 h. After then, the organic layer was separated, dried over anhydrous Na₂SO₄ and filtered. The filtrate was evaporated to dryness and the residue was purified by silica gel column chromatography eluting with a mixture of EA and hexane (3:1) to afford the products (pypy)H and (pmpy)H, respectively.

Selected data of (pypy)H. Yellow oil, yield: 72%. MS (EI): *m/z* 272.2 (M⁺). ¹H NMR (400 MHz, CDCl₃, 298 K): δ 8.53 (d, *J* = 5.2 Hz, 1H), 8.18 (d, *J* = 8.4 Hz, 1H), 7.92 (s, 1H), 7.45 (dd, *J* = 5.2 Hz, 1H), 6.23 (d, *J* = 8.4 Hz, 1H), 4.02 (s, 3H), 3.96 (s, 3H), 1.33 (s, 9H).

Selected data of (pmpy)H. Yellow oil, yield: 56%. MS (EI): *m/z* 273.2 (M⁺). ¹H NMR (400 MHz, CDCl₃, 298 K): δ 8.80 (s, 1H), 8.55 (d, *J* = 5.2 Hz, 1H), 7.76 (s, 1H), 7.21 (dd, *J* = 5.2 Hz, 1H), 4.06 (s, 3H), 4.03 (s, 3H), 1.33 (s, 9H).

Preparation of dimer [Ir(C[^]N)₂(μ-Cl)]₂. A suspension of [Ir(cod)(μ-Cl)]₂ (1.0 equiv.) and the respective ligand (C[^]N = pypy, pmpy; 4.1 equiv.) in 2-ethoxyethanol (15 mL) was heated at 140 °C for 6 h. After cooled to RT, excess of methanol was added to induce precipitation. The resulting precipitate was filtered, washed with methanol and hexane in sequence. The dimers [Ir(C[^]N)₂(μ-Cl)]₂ were obtained in high purity and used without further purification.

Preparation of Ir(III) metal complexes. A suspension of [Ir(C[^]N)₂(μ-Cl)]₂ (C[^]N = pypy, pmpy; 1.0 equiv.), ancillary ligand (PzH or PrH, 2.1 equiv.) and Na₂CO₃ (10.0 equiv.) in 2-methoxyethanol (15 mL) was heated at 125 °C for 4 h. After then, excess

of deionized water was added to induce precipitation. The resulting precipitate was filtered, washed with methanol and hexane in sequence. After chromatographic separation and recrystallization, the corresponding Ir(III) complexes [Ir(C^N)₂(L^X)] (C^N = pypy, pmpy; L^X = Pz, Pr) was obtained as pale yellow solid.

Ir(pypy)₂(Pz) (1). Pale yellow solid, yield: 84%. MS (FAB, ¹⁹³Ir): m/z 1003.7 (M⁺). ¹H NMR (400 MHz, CDCl₃, 298 K): δ 8.52 (s, 1H), 8.43 (s, 1H), 7.66 (d, J = 6.0 Hz, 1H), 7.63 (s, 1H), 7.39 (d, J = 6.0 Hz, 1H), 7.24 (d, J = 6.4 Hz, 1H), 6.96 (dd, J = 6.0 Hz, 1H), 6.92 (s, 1H), 6.86 (dd, J = 6.0 Hz, 1H), 6.72 (dd, J = 6.4 Hz, 1H), 5.37 (s, 1H), 5.27 (s, 1H), 4.04 (s, 3H), 4.00 (s, 3H), 3.77 (s, 3H), 3.71 (s, 3H), 1.30 (m, 27 H). ¹⁹F-¹H NMR (470 MHz, CDCl₃, 298 K): δ -59.73 (s, 3F). Anal. calcd. for C₄₅H₅₁F₃IrN₇O₄: N, 9.77; C, 53.88; H, 5.12%. Found: N, 9.88; C, 53.76; H, 5.5%.

Ir(pypy)₂(Pr) (2). Pale yellow solid, yield: 76%. MS (FAB, ¹⁹³Ir): m/z 1070.7 (M⁺). ¹H NMR (400 MHz, CDCl₃, 298 K): δ 8.51 (s, 1H), 8.45 (s, 1H), 8.08 (s, 1H), 7.60 (d, J = 6.0 Hz, 1H), 7.56 (d, J = 6.0 Hz, 1H), 7.15 (d, J = 6.4 Hz, 1H), 6.84 (m, 3H), 6.74 (dd, J = 6.4 Hz, 1H), 5.21 (s, 1H), 5.16 (s, 1H), 4.04 (s, 3H), 4.01 (s, 3H), 3.76 (s, 3H), 3.68 (s, 3H), 1.32 (m, 18H), 1.29 (s, 9H). ¹⁹F-¹H NMR (470 MHz, CDCl₃, 298 K): δ -54.68 (s, 3F), -58.74 (s, 3F). Anal. calcd. for C₄₇H₅₁F₆IrN₆O₄: N, 7.85; C, 52.75; H, 4.80%. Found: N, 7.88; C, 52.73; H, 5.14%.

Ir(pmpy)₂(Pz) (3). Pale yellow solid, yield: 93%. MS (FAB, ¹⁹³Ir): m/z 1005.5 (M⁺). ¹H NMR (400 MHz, CDCl₃, 298 K): δ 8.29 (s, 1H), 8.23 (s, 1H), 7.71 (d, J = 6.0 Hz, 1H), 7.67 (s, 1H), 7.57 (d, J = 6.4 Hz, 1H), 7.45 (d, J = 6.0 Hz, 1H), 7.01 (dd, J = 6.0 Hz, 1H), 6.96 (s, 1H), 6.91 (dd, J = 6.0 Hz, 1H), 6.81 (dd, J = 6.4 Hz, 1H), 4.04 (s, 3H), 4.00 (s, 3H), 3.53 (s, 3H), 3.41 (s, 3H), 1.33 (s, 9H), 1.29 (m, 18H). ¹⁹F-¹H NMR (470 MHz, CDCl₃, 298 K): δ -59.77 (s, 3F). Anal. calcd. for C₄₃H₄₉F₃IrN₉O₄: N, 12.54; C, 51.38; H, 4.91%. Found: N, 12.29; C, 51.84; H, 5.31%.

Ir(pmpy)₂(Pr) (4). Pale yellow solid, yield: 63%. MS (FAB, ¹⁹³Ir): m/z 1072.7 (M⁺). ¹H NMR (400 MHz, CDCl₃, 298 K): δ 8.28 (s, 1H), 8.23 (s, 1H), 8.12 (s, 1H), 7.65 (m, 2H), 7.36 (d, J = 6.4 Hz, 1H), 6.90 (m, 2H), 6.86 (s, 1H), 6.82 (dd, J = 6.4 Hz, 1H), 4.04 (s, 3H), 4.00 (s, 3H), 3.48 (s, 3H), 3.34 (s, 3H), 1.32 (s, 9H), 1.29 (m, 18H). ¹⁹F-¹H

NMR (470 MHz, CDCl₃, 298 K): δ -54.75 (s, 3F), -59.33 (s, 3F). Anal. calcd. for C₄₅H₄₉F₆IrN₈O₄: N, 10.45; C, 50.41; H, 4.61%. Found: N, 10.39; C, 50.53; H, 4.61%.

Single Crystal X-Ray Diffraction Studies. Single crystal X-ray diffraction data were measured on a Bruker SMART Apex CCD diffractometer using Mo radiation ($\lambda = 0.71073$ Å). The data collection was executed using the *SMART* program. Cell refinement and data reduction were performed with the *SAINTE* program. An empirical absorption was applied based on the symmetry-equivalent reflections and the *SADABS* program. The structures were solved using the *SHELXS-97* program and refined using *SHELXL-97* program by full-matrix least squares on F^2 values. The structural analysis and molecular graphics were obtained using *SHELXTL* program on PC computer.³⁸ CCDC-1042596 and 1038961 contain the supplementary crystallographic data for this paper. These data can be obtained free of charge from the Cambridge Crystallographic Data Centre via <http://www.ccdc.cam.ac.uk>.

Selected crystal data of **3**: C₄₃H₄₉F₃IrN₉O₄; M = 1005.11; T = 200(2) K; $\lambda(\text{Mo-K}\alpha) = 0.71073$ Å; triclinic; space group = *P*-1; $a = 15.2000(8)$, $b = 15.4108(8)$, $c = 16.1956(8)$ Å, $\alpha = 63.7115(9)^\circ$, $\beta = 64.9839(10)^\circ$, $\gamma = 81.0448(10)^\circ$; $V = 3079.9(3)$ Å³; $Z = 2$; $\rho_{\text{calcd}} = 1.084$ Mg·m⁻³; $\mu = 2.213$ mm⁻¹; $F(000) = 1012$; crystal size = $0.34 \times 0.24 \times 0.14$ mm³; 39783 reflections collected, 14052 independent reflections ($R_{\text{int}} = 0.0314$), max. and min. transmission = 0.7469 and 0.5564, restraints / parameters = 96 / 578, GOF = 1.042, final $R_1[I > 2\sigma(I)] = 0.0284$ and $wR_2(\text{all data}) = 0.0741$.

Selected crystal data of **4**: C₄₅H₄₉F₆IrN₈O₄; M = 1115.21; T = 150(2) K; $\lambda(\text{Mo-K}\alpha) = 0.71073$ Å; triclinic; space group = *P*-1; $a = 12.8914(5)$, $b = 13.0578(5)$, $c = 15.8885(6)$ Å, $\alpha = 106.7420(10)^\circ$, $\beta = 96.0820(10)^\circ$, $\gamma = 99.5340(10)^\circ$; $V = 2492.16(17)$ Å³; $Z = 2$; $\rho_{\text{calcd}} = 1.486$ Mg·m⁻³; $\mu = 2.751$ mm⁻¹; $F(000) = 1126$; crystal size = $0.34 \times 0.15 \times 0.12$ mm³; 32464 reflections collected, 11416 independent reflections ($R_{\text{int}} = 0.0411$), max. and min. transmission = 0.7337 and 0.4548, restraints / parameters = 201 / 623, GOF = 1.098, final $R_1[I > 2\sigma(I)] = 0.0337$ and $wR_2(\text{all data}) = 0.0815$.

TD-DFT Calculation All calculations were performed by Gaussian 09 program.³⁹ The B3LYP density functional theory (DFT)^{40, 41} which combines the Becke's three-parameter hybrid exchange theory and the Lee-Yang-Parr correlation theory was used to optimize the structures in the ground state for complexes **1** - **4**. Based on the optimized geometrical structure in the ground state, 100 singlet and 6 triplet excited states were calculated to determine the vertical excitation energies by time-dependent density functional theory (TD-DFT). Moreover, for determining the phosphorescence, geometries of these complexes in the lowest-energy triplet state T_1 were also optimized. Then 6 triplet excited states were calculated on the base of optimized T_1 states. In these calculations, a polarizable continuum model (PCM) using CH_2Cl_2 solvent was applied.^{42, 43} The Stuttgart-Dresden (SDD)⁴⁴ basis set and the effective core potentials (ECPs) was used to describe the Ir atom. Other non-metal atoms of F, O, N, C and H were described by the all-electron basis set of 6-31G*. Visualization of the frontier molecular orbitals were performed by GaussView.

OLED device fabrications. All materials were purified by vacuum sublimation prior to use. The OLEDs were fabricated through direct vacuum deposition at 10^{-6} torr on the ITO-coated glass substrates having a sheet resistance of $15 \Omega \text{ sq}^{-1}$. The ITO surface was ultrasonically cleaned in acetone, methanol and deionized water in sequence, followed by a final treatment with air plasma. The deposition rate was kept at ca. $1 - 2 \text{ \AA s}^{-1}$. Subsequently, LiF was deposited at 0.1 \AA s^{-1} and then capped with Al metal (ca. 5 \AA s^{-1}) through shadow masking without breaking the vacuum. The $J-V-L$ characteristics of the devices were measured simultaneously in a glove-box using a Keithley 6430 source meter and a Keithley 6487 picoammeter equipped with a calibration Si-photodiode. EL spectra were measured using a photodiode array (Ocean Optics USB2000+).

Results and Discussion

Synthesis and characterization. The wide band-gap cyclometalating chelates, i.e.

4-*t*-butyl-2',6'-dimethoxy-2,3'-bipyridine, (pypy)H and 2-(2,4-dimethoxypyrimidin-5-yl)-4-*t*-butylpyridine, (pmpy)H, are synthesized using the Pd-catalyzed Suzuki-Miyaura cross-coupling involving 4-*t*-butyl-2-chloropyridine and 2,6-dimethoxypyridine-3-boronic acid (or 2,4-dimethoxypyrimidine-5-boronic acid), according to the modified literature procedures.^{45,46} Next, the Ir(III) complexes were constructed by the typical two-step procedure, which involved treatment of (pypy)H and (pmpy)H chelates with [Ir(cod)(μ -Cl)]₂ to afford the corresponding Ir(III) dimers [(pypy)₂Ir(μ -Cl)]₂ and [(pmpy)₂Ir(μ -Cl)]₂, according to the method reported by Baranoff and coworkers,²⁶ followed by addition of 2-[3-(trifluoromethyl)-1*H*-pyrazol-5-yl]-4-*t*-butyl-pyridine (PzH) and 2-[3,5-bis(trifluoromethyl)-1*H*-pyrrol-2-yl]-4-*t*-butyl-pyridine (PrH) at elevated temperature. This protocol has afforded the desired Ir(III) metal complexes, i.e. Ir(pypy)₂(Pz) (**1**), Ir(pypy)₂(Pr) (**2**), Ir(pmpy)₂(Pz) (**3**) and Ir(pmpy)₂(Pr) (**4**), in high yields and high purity. Their identities are initially confirmed by spectroscopic analyses, such as mass spectrometry and NMR, and by elemental analysis.

Single-crystal X-ray diffraction studies on both **3** and **4** were carried out to reveal their exact coordinative arrangement. As indicated in Figures 1 and 2, their molecular structures consist of a slightly distorted octahedral geometry, similar to the geometry displayed by relevant heteroleptic Ir(III) complexes.⁴⁷⁻⁵⁰ The pmpy chelates show *trans*-Ir-N bond lengths of 2.039(2) and 2.041(2) Å in **3** and 2.037(3) and 2.044(3) Å in **4**, which are all within the normal ranges expected for analogous cyclometalated Ir(III) complexes. The carbon donor atoms, e.g. C(1) and C(16) for **3** and C(22) and C(37) for **4**, are *cis* to one another, for which their respective Ir-C distances, 1.970(2) and 1.982(3) Å, 1.972(3) and 1.989(4) Å are also comparable to those of the heteroleptic Ir(III) complexes with dual cyclometalating chelates such as in [Ir(dfppy)₂(Pz)],⁵¹ [(tfmppy)₂Ir(tpip)],⁵² [Ir(ppy)₂(PyTz)]⁵³ and FK306.⁵⁴ The Pz and Pr metallacycles in **3** and **4** are planar; however, the Ir-N distance to the pyrazolate fragment in **3** (Ir-N(8) = 2.118(2) Å) is found to be notably shorter than that of the pyrrolide fragment in **4** (Ir-N(2) = 2.155(3) Å), despite of having similar Ir-N distance

to the nearby pyridinyl fragment, c.f. Ir-N(7) = 2.159(2) and Ir-N(1) = 2.151(3) Å. This observation suggests the existence of stronger dative bonding interaction between Ir(III) atom and pyrazolate versus pyrrolide, which could be, in part, attributed to the larger steric encumbrance imposed by the adjacent CF₃ group of pyrrolide.^{55, 56}

Photophysical properties. Absorption and emission spectra recorded in CH₂Cl₂ solution are compiled in Figure 3 and the corresponding numeric data are summarized in Table 1. All Ir(III) complexes **1** – **4** showed broadened absorption at approx. 345 nm that can be assigned to spin-allowed ligand-centered ¹ππ* transitions of the chromophoric cyclometalates, which partially overlap with spin-allowed ¹ππ* transition of the Pz or Pr ancillary. Only minor spectral change was observed upon variation of either cyclometalate chelates (i.e. pypy and pmpy) or ancillaries (i.e. Pz and Pr) in the present system. However, the less intense shoulder at approx. 370 nm are probably due to spin-allowed ¹MLCT transitions. These ¹MLCT peaks are difficult to be resolved due to the tailing of ¹ππ* transition, for which the lower absorptivities are attributed to the poor spatial overlap between the d_π orbitals of central Ir(III) metal atom and π* orbitals of chelates.

The PL spectra in degassed CH₂Cl₂ were next recorded which are also shown in Figure 3. Great variation of intensity between aerated and degassed solution were observed for all Ir(III) metal complexes, ensures that the emission is originating from the triplet manifold, i.e. the phosphorescence. The radiative and non-radiative decay rate constants were calculated using the equations: $k_r = \Phi/\tau_{obs}$ and $k_{nr} = 1/\tau_{obs} - k_r$. As showed in Table 1, radiative decay rate constants k_r of 1.03 – 2.10 × 10⁵ s⁻¹ were deduced for Ir(III) complexes **1** – **4**. Since these heteroleptic structures with pyridyl azolate or pyrrolide ancillary are considered to be more rigid than that of the analogous Ir(III) complexes with picolinate ancillary,¹⁶ a major radiationless deactivation associated with large amplitude skeletal motion seems to be unlikely, which accounts for the reduced non-radiative decay rate constants observed between them.

Moreover, both pypy complexes **1** and **2** showed essentially identical spectral

pattern, with two peak maxima at 458 and 489 nm and a less intense shoulder in the longer wavelength region. The occurrence of these vibronic envelopes reflected the strong influence from the $^3\pi\pi$ excited states, together perhaps with minor contribution from the $^3\text{MLCT}$ excited states. In sharp contrast, emission for **3** is significantly blue-shifted, showing peak maxima at 444 and 472 nm, for which the E_{0-0} transition is approx. blue-shifted by 14 nm versus that of the ppy complexes **1** and **2**. This observation is in agreement with the larger ligand-centered $\pi\pi^*$ gap for pmpy chelates versus that of the corresponding ppy chelates. In sharp contrast to **3**, the second pmpy complex, i.e. Ir(III) complex **4** with the pyrrolide based ancillary (i.e. Pr), reveal a different emission profile, for which the intensity of E_{0-0} transition is slightly suppressed, together with concomitant increase in intensity for the longer wavelength shoulders. Such a change of emission pattern seems to be not coming from impurity in solid sample, as the spectral profile remained unaltered even after repeated separation using both chromatography and recrystallization. Furthermore, this broadened spectral profile offsets the endeavor for inducing the blue-shifting of luminescence, making this complex less ideal to serve the monochromic blue phosphor.

Electrochemistry. The electrochemical properties of **1** – **4** were examined using cyclic voltammetry. In contrast to the typical Ir(III) complexes with reversible metal-centered oxidation and irreversible ligand-centered reduction processes, these Ir(III) complexes **1** – **4** showed irreversible oxidation onset at 0.94, 0.93, 1.06 and 1.07 V in CH_2Cl_2 (vs. the ferrocenium/ferrocene couple at 0.0 V, c.f. Figure SE of electronic supporting information), whilst the reduction peak was not detectable up to the limit of -3.0 V. The alternation in oxidation onsets followed the anticipation based on the greater electron deficient character of the pmpy versus ppy chelates. Furthermore, it is expected that the Pr ancillary in **2** and **4** would reduce the negative charge density at the metal and, then, exhibit a slightly increased onset.

Theoretical calculation. DFT/TD-DFT calculations were also performed to study

the detailed photophysical properties of complexes **1** – **4** in CH₂Cl₂ solution. The calculated lowest-energy absorption wavelength of S₁ states, primarily coming from the transitions of HOMO → LUMO/LUMO+1, are 358, 362, 351 and 362 nm, respectively, for complexes **1** – **4** (Table 2), which are close to the experimental absorption onsets (Figures S1, S3, S5, S7). From the analysis of orbital components (Figure 4), it can be found that the HOMO are mainly distributed in the chromophoric cyclometalates (pypy for complexes **1** and **2**; pmpy for complexes **3** and **4**) with the contributions of 77%, 81%, 65% and 43% and d orbital of Ir atom with the contributions of 20%, 17%, 32% and 26%, respectively, except for complex **4** with some important distribution in Pr ancillary (32%). The LUMO/LUMO+1 orbitals are primarily located on the pypy/pmpy and Pz/Pr ligands with no less than 92% contributions. So the transitions from their ground states to the S₁ states are ascribed to the predominant intra-ligand (¹IL) [$\pi \rightarrow \pi^*$ (pypy/pmpy)] transitions with moderate [π (pypy/pmpy) → π^* (Pz/Pr)] ligand-to-ligand charge transfer (¹LLCT), combined with minor [d_{π} (Ir) → π^* (Pz/Pr)] metal-to-ligand charge transfer (¹MLCT) character. The second, higher energy absorption was calculated to locate at 314, 314, 317 and 336 nm, which are corresponding to the experimental absorption peaks observed at 328, 332, 338 and 338 nm for complexes **1** – **4**, respectively, and their characteristics can be mainly assigned to the ¹IL $\pi\pi^*$ transition in chromophoric cyclometalates according to the transition component and orbital distribution (see Supporting Information for more details).

Moreover, the calculated wavelengths of the lowest-energy triplet states T₁ in the optimized structures of ground state S₀ are estimated to locate at 433, 438, 418 and 437 nm, respectively (Table 2), which agree with the experimentally observed lowest-energy absorption band in the region of 380-440 nm. The variation is also consistent with the trend of phosphorescence spectra, with the greatest blue shift for complex **3** by comparison with that observed for all other Ir(III) complexes. The properties of first three lowest-energy triplet states T₁ – T₃ for complexes **1** – **4** and the corresponding assignment are detailed in Tables S1 - S4. Combining with the

orbital distribution (Figures S2, S4, S6, S8, Supporting Information), it can be found that the transition are primarily ascribed to the contribution from intra-ligand charge transition ${}^3\text{IL}$. It is noted that the calculated transition probability (oscillator strength, f) from S_0 to T_n ($n = 1 - 3$) is zero owing to the forbidden singlet-triplet transition under the TD-DFT calculation in Gaussian program without considering the spin-orbit coupling. But for these Ir(III) complexes, the transition from S_0 to T_n should be partly allowed as a result of the larger spin-orbit coupling induced by the heavy Ir(III) metal atom.

Based on the optimized geometrical structures of T_1 states which were treated as the reference states, the triplet excitation transition were also calculated. The electron density difference (EDD) of $\Delta\rho(T_1-S_0)$ between the first triplet excited state T_1 and ground state S_0 in the optimized T_1 state in CH_2Cl_2 solution were displayed in Figure 5. It is obvious that the electron are primarily excited to the chromophoric cyclometalates (pypy/pmpy), while the hole are left on the same parts but with different regions and on the Ir(III) metal atom. Accordingly, we can deduce that the phosphorescence are mainly derived from the intra-ligand $\pi\pi^*$ transition within the cyclometalating pypy/pmpy chelates, combined with some $[d_\pi(\text{Ir}) \rightarrow \pi^*(\text{pypy/pmpy})]$ ${}^3\text{MLCT}$ character. The spin-density distribution of the triplet state also confirm this conclusion, c.f. the right column of Figure 5.

Electroluminescent Devices. PhOLEDs were fabricated using the Ir(III) complexes **1 – 4** as dopants in device architecture with double-emission-layers (DEL): indium tin oxide (ITO)/ HAT-CN (10 nm)/ DTAF (40 nm)/ TCTA (10 nm)/ CaSi: 8% dopant (10 nm)/ POCz3: 8% dopant (15 nm)/ 3TPYMB (50 nm)/ LiF (0.5 nm)/ Al (100 nm). The DEL comprises two different host materials that have higher triplet excited state than that of dopant and opposite carrier-transporting property in order to bring about a better balance between the electron and hole-transport.^{14, 57} Figure 6 shows the schematic diagram of the device structure and the molecular drawings of materials used in the device. To improve the hole injection from the anode, we used 4,5,8,9,11-hexaazatriphenylene-hexacarbonitrile (HAT-CN)⁵⁸ as the hole injection

layer. Two hole transport layers (HTLs), which consisted of a 40-nm-thick layer of 9,9-di[4-(di-*p*-tolyl)aminophenyl]fluorene (DTAF)⁵⁹⁻⁶¹ and a 10-nm-thick layer of 4,4',4''-tri(*N*-carbazolyl)triphenylamine (TCTA)^{62, 63} were implemented. It is noteworthy that TCTA (HOMO = -5.7 eV) was inserted between DTAF and CaSi to show a stepwise increase in HOMOs into the emitting layer. The DEL consists of two hosts, both are doped with 8 % of Ir(III) phosphors; one is the hole transporting diphenylbis[4-(9-carbazoyl)phenyl]silane (CaSi),⁶⁴ while the second is the electron transporting 3,3',3''-phosphoryl tris(9-phenyl-9Hcarbazole) (POCz3, 15 nm).⁶⁵ For effectively confining the excitons, tris-[3-(3-pyridyl)mesityl]borane (3TPYMB)⁶⁶⁻⁶⁸ with a high triplet-energy gap (E_T : 2.98 eV and HOMO/LUMO: 6.8/3.3 eV) was employed as the electron-transporting layer (ETL). The device was completed using LiF and Al as electron-injecting layer and cathode, respectively.

Figure 7 depicts the current density-voltage-luminance (*J-V-L*) characteristics, device efficiencies, and EL spectra of the device. The key characteristics of the devices are listed in Table 3. The electroluminescence (EL) spectra consist only of a blue phosphor emission without any residual emission from the host and/or adjacent layers, even at high drive currents – an indication of complete energy and/or charge transfer from the host exciton to the phosphor upon electrical excitation. There is a close resemblance between the EL and PL spectra in each case. The turn-on voltage of all devices are recorded to be 3.0 V owing to the good matching of HOMO and LUMO energy levels between hole and electron transporting materials and Ir(III) dopants. The **2** doped blue PhOLED reveals a max. brightness (L_{max}) of 17050 cd/m² at 13.0 V (950 mA/cm²) with the CIE coordinates of (0.16, 0.24). The max. external quantum (η_{ext}), current (η_c), and power efficiencies (η_p) were 14.3 %, 23.8 cd/A, and 18.2 lm/W, respectively, which are resemble to those of blue-emitting Ir(III) complexes documented.^{50, 69-72} At the practical brightness of 1000 cd/m², the external quantum efficiency drop to about 10.8 %. These efficiency roll-offs are to be expected for phosphorescent OLEDs at higher current densities.^{73, 74} Device **1** has almost the same EL spectra with emission maxima at 459 and 488 nm as well as a

slightly lower device efficiencies (9.0 %, 14.5 cd/A, and 12.7 lm/W) as a consequence of the longer radiation lifetime (7.7 μ s) and versus that of dopant **2** (6.2 μ s) recorded under similar condition.

In addition, the **4** and **3** phosphors, both adopt 5-pyridin-2-yl-pyrimidine chelates, display further blue-shifted emission (456 and 475 nm) compared to the 2,3'-bipyridine based phosphors **2** and **1** due to the enlarged gap. The device with dopant **4** reveals a max. brightness (L_{\max}) of 9550 cd/m² at 13.5 V (1240 mA/cm²) with the CIE coordinates of (0.16, 0.20). Its max. efficiencies were recorded to be 9.4 %, 14.4 cd/A and 11.5 lm/W, which are significantly higher than those for the device **3** (5.8 %, 7.9 cd/A and 7.1 lm/W), which showed the best true-blue CIE coordinates of (0.16, 0.17) among all phosphors.

Conclusion

In summary, we have shown the successful preparation of blue-emitting Ir(III) phosphors **1** – **4**, bearing the fluorine-free ppy and pmpy chromophoric chelates. The photophysical studies showed the existence of intense, structured blue phosphorescence with E_{0-0} peak (\leq 458 nm) and higher quantum yield (\geq 79 %) in solution, for which the recorded emission characteristics are comparable to those of the best Ir(III) phosphors with 4,6-difluorophenylpyridinato cyclometalates documented in literature. According to the DFT/TD-DFT studies, the electron withdrawing nitrogen atom(s) of the cyclometalating segments are capable to stabilize the π -orbital of the chelates and, in the meantime, the respective methoxy fragments provide a dual function in lowering the d_{π} electron density at the Ir(III) center and increasing the π^* -energy level of chelates. Thus, the synergy of nitrogen atoms and methoxy groups is clearly the main factor that produced the blue-shifted emission. As for the OLED applications, ppy phosphor **2** showed the highest efficiency characteristics, i.e. max. external quantum (η_{ext}), current (η_c), and power efficiencies (η_p) of 14.3 %, 23.8 cd/A, and 18.2 lm/W, respectively. Moreover, the associated η_{ext} was only dropped to 10.8 % at 1000 cd/m², and showing blue CIE_{x,y}

color coordinates of (0.16, 0.24) at 100 cd/m², versus the CIE_{x,y} coordinates of (0.16, 0.17), as showed by the phosphor **3**. These results underline the great potential of these Ir(III) complexes in both the synthetic organometallic chemistry as well as the application as alternative phosphors for OLED studies.

Acknowledgments. This work was supported by the Ministry of Science and Technology of Taiwan, under the grant NSC-101-2113-M-007-013-MY3.

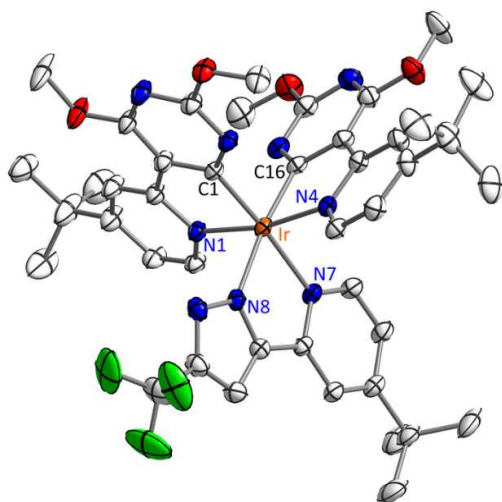


Figure 1. Structural drawing of **3** with thermal ellipsoids shown at 30% probability level, selected bond distances: Ir-N(1) = 2.039(2), Ir-N(4) = 2.041(2), Ir-N(8) = 2.118(2), Ir-N(7) = 2.159(2), Ir-C(1) = 1.970(2) and Ir-C(16) = 1.982(3) Å; selected bond angles N(7)-Ir-C(1) = 175.48(9), N(8)-Ir-C(16) = 172.34(8) and N(1)-Ir-N(4) = 168.68(8)°.

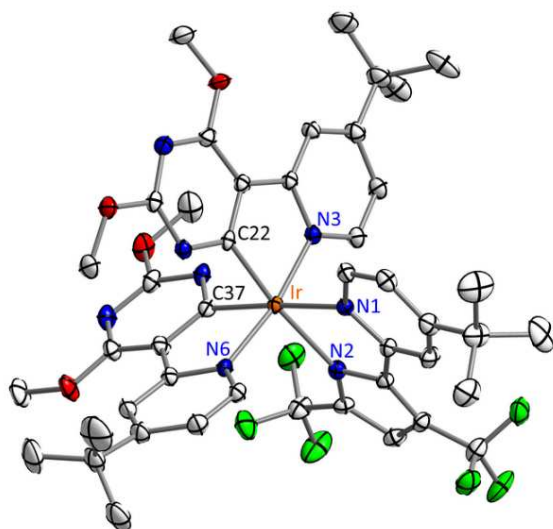


Figure 2. Structural drawing of **4** with thermal ellipsoids shown at 30% probability level, selected bond distances: Ir-N(1) = 2.151(3), Ir-N(2) = 2.155(3), Ir-N(3) = 2.037(3), Ir-N(6) = 2.044(3), Ir-C(22) = 1.972(3) and Ir-C(37) = 1.989(4) Å; selected bond angles N(1)-Ir-C(37) = 174.81(12), N(2)-Ir-C(22) = 172.16(12) and N(3)-Ir-N(6) =

170.32(11)°.

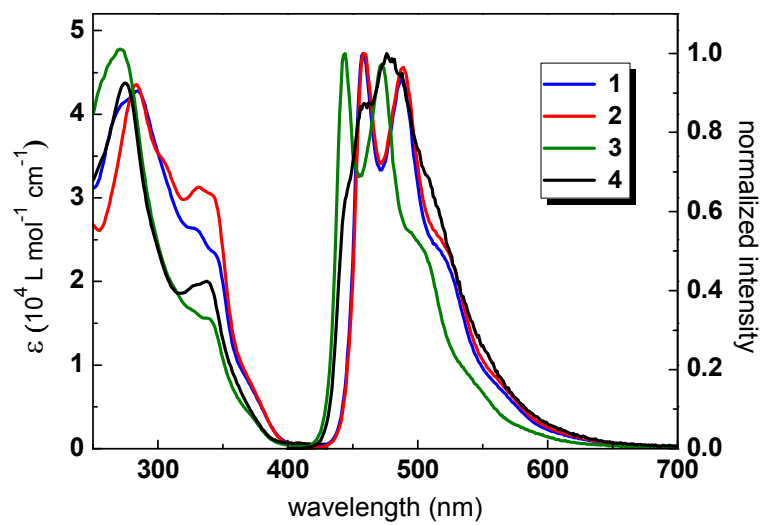


Figure 3. Absorption and normalized emission spectra of complexes **1** – **4** in degassed CH_2Cl_2 at RT.

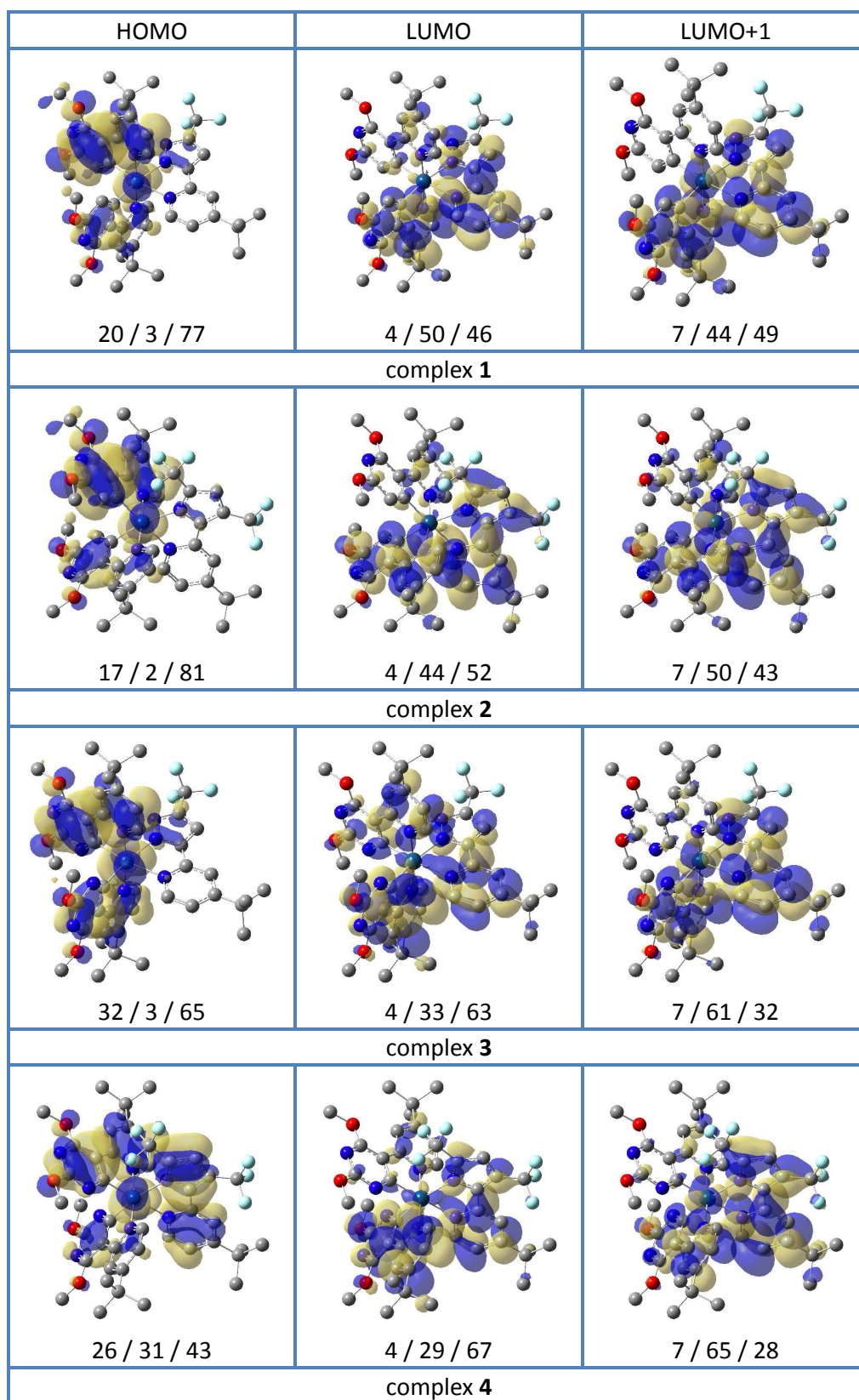


Figure 4. Plots of the selected frontier orbitals involved in the transitions of S_1 states for complexes **1** - **4** in CH_2Cl_2 solution calculated by TD-DFT method at the B3LYP level (isovalue = 0.02), combined with the orbital compositions of Ir metal / Pz or Pr / pypy or pmpy fragment in percentile (%). The blue and yellow parts represent different phases, respectively.

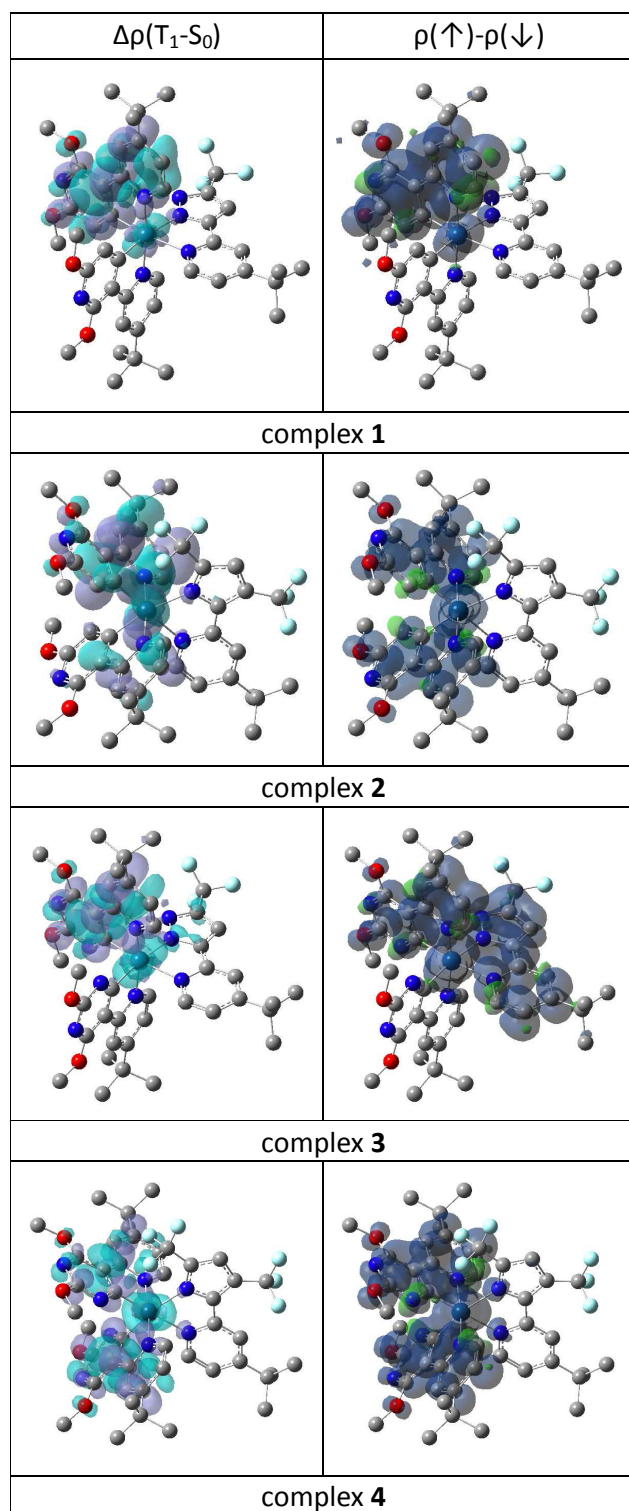


Figure 5. Plots of electron density difference (EDD) of $\Delta\rho(T_1-S_0)$ (isovalue = 0.02) and

spin density (SD) of $\rho(\uparrow)-\rho(\downarrow)$ (isovalue = 0.0008) in the optimized T_1 state for **1** – **4** in CH_2Cl_2 . The light blue and purple colors of EDD images represent the electron depletion (ED) and electron accumulation (EA) region, respectively; while the dark blue and green parts of SD images represent the net electron distribution of spin up and spin down, respectively.

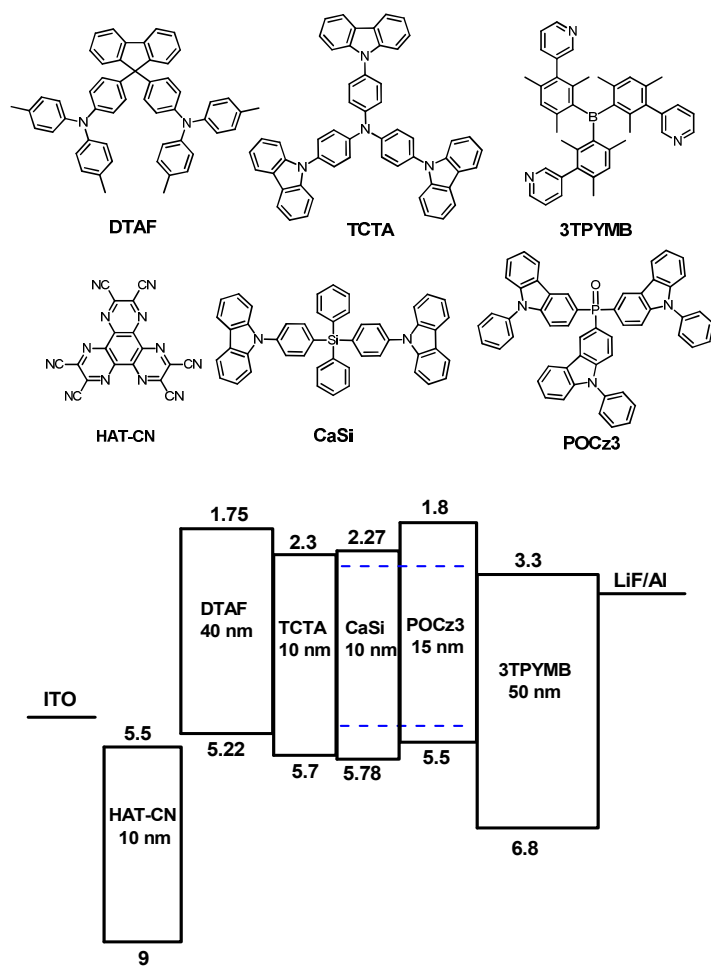


Figure 6. Molecular structures of materials used in this study and an energy level diagram of the device.

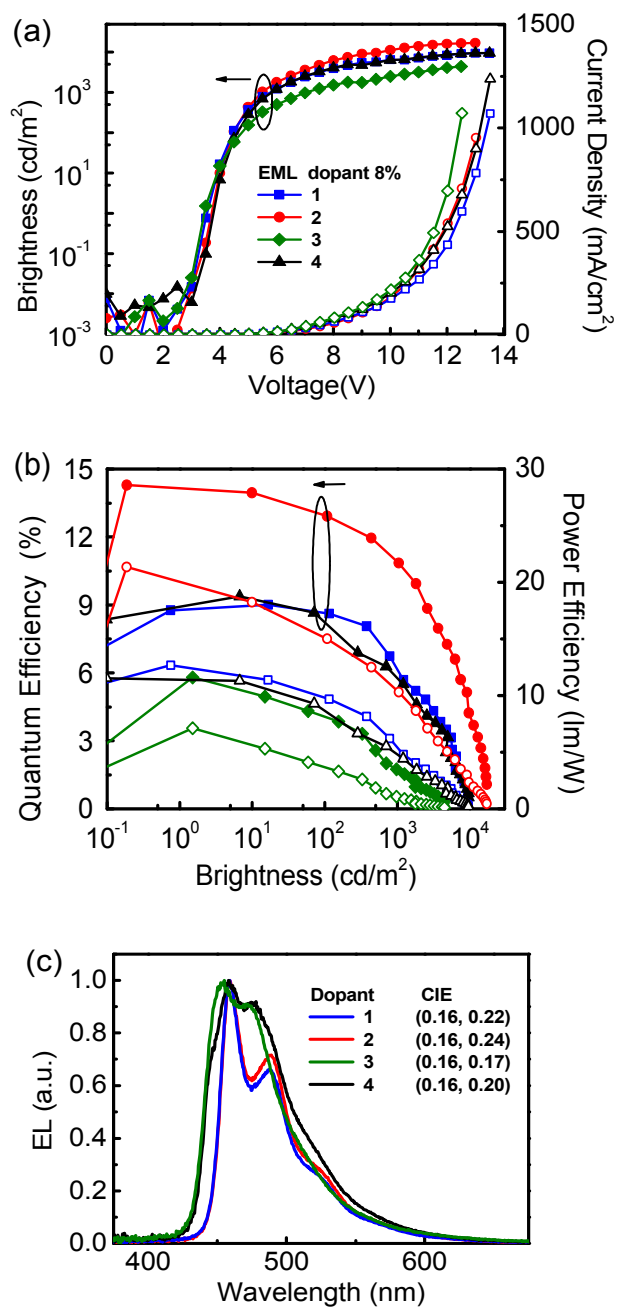


Figure 7. (a) Current density-voltage-luminance (J - V - L) characteristics, (b) external quantum (η_{ext}) and power efficiencies (η_p) as a function of brightness, and (c) EL spectra for devices incorporating Ir(III) metal dopants.

Table 1. Photophysical data of the studied Ir(III) complexes recorded in CH₂Cl₂ at RT.

	λ_{abs} (nm) / ϵ ($10^4 \text{ M}^{-1}\text{cm}^{-1}$)	λ_{em} (nm)	Φ^{b}	τ (μs) ^b	k_{r} (s^{-1})	k_{nr} (s^{-1})
1	283 / 4.3, 328 / 2.6	458, 488, 510 ^a	0.79	7.7	1.03×10^5	2.7×10^4
2	283 / 4.4, 332 / 3.1	458, 489, 510 ^a	0.79	6.2	1.27×10^5	3.4×10^4
3	271 / 4.8, 338 / 1.6	444, 472, 493 ^a	0.91	4.2	2.17×10^5	2.1×10^4
4	275 / 4.4, 338 / 2.0	458, 476, 507 ^a	0.93	6.0	1.55×10^5	1.2×10^4

^a shoulder peak.

^b The quantum yields were measured in degassed CH₂Cl₂ and with coumarin102 ($\Phi = 0.87$ in methanol) as reference.

Table 2. The calculated energy levels and orbital transition analyses for complexes **1**

– 4.

	State	λ nm (eV)	f	transitions	assignment	MLCT%
1	S ₁	358 (3.46)	0.0545	HOMO → LUMO (59%) HOMO → LUMO+1 (17%)	¹ IL/ ¹ LLCT/ ¹ MLCT ¹ IL/ ¹ LLCT/ ¹ MLCT	15%
	T ₁	433 (2.86)	0.0000	HOMO→LUMO+2 (28%) HOMO→LUMO (15%) HOMO-1→LUMO+1 (13%) HOMO-1→LUMO+2 (12%)	³ IL/ ³ MLCT ³ IL/ ³ LLCT/ ³ MLCT ³ IL/ ³ LLCT ³ IL	11%
2	S ₁	362 (3.43)	0.0451	HOMO→LUMO (47%) HOMO→LUMO+1 (30%)	¹ IL/ ¹ LLCT/ ¹ MLCT ¹ IL/ ¹ LLCT/ ¹ MLCT	12%
	T ₁	438 (2.83)	0.0000	HOMO-1→LUMO+1 (42%) HOMO-1→LUMO (40%)	³ IL/ ³ LLCT ³ IL/ ³ LLCT	1%
3	S ₁	351 (3.53)	0.0705	HOMO→LUMO (76%) HOMO→LUMO+1 (14%)	¹ IL/ ¹ MLCT ¹ LLCT/ ¹ IL/ ¹ MLCT	28%
	T ₁	418 (2.97)	0.0000	HOMO→LUMO (33%) HOMO-2→LUMO+2 (13%) HOMO→LUMO+2 (12%) HOMO→LUMO+1 (11%)	³ IL/ ³ MLCT ³ IL/ ³ LLCT ³ IL/ ³ MLCT ³ LLCT/ ³ IL/ ³ MLCT	23%
4	S ₁	362 (3.42)	0.0253	HOMO→LUMO (63%) HOMO→LUMO+1 (20%)	¹ IL/ ¹ MLCT ¹ IL/ ¹ MLCT/ ¹ LLCT	21%
	T ₁	437 (2.84)	0.0000	HOMO-1→LUMO+1 (39%) HOMO→LUMO+1 (32%)	³ IL ³ IL/ ³ MLCT/ ³ LLCT	10%

Table 3. EL performance of devices incorporating different Ir(III) dopants at 8 wt.%.

	V_{on} [V] ^a	max. L [cd/m ²]	max. η_i [mA/cm ²]	max. η_{ext} [% , cd/A]	max. η_p [lm/W]	[% , V] at 10 ³ cd/m ²	CIE [x,y]
1	3.0	9530 (13.5 V)	1070	9.0, 14.5	12.7	6.3, 5.6	0.16, 0.22
2	3.0	17050 (13.0 V)	950	14.3, 23.8	18.2	10.8, 5.5	0.16, 0.24
3	3.0	4440 (12.5V)	1070	5.8, 7.9	7.1	1.7, 7.0	0.16, 0.17
4	3.0	9550 (13.5 V)	1240	9.4, 14.4	11.5	5.7, 5.8	0.16, 0.20

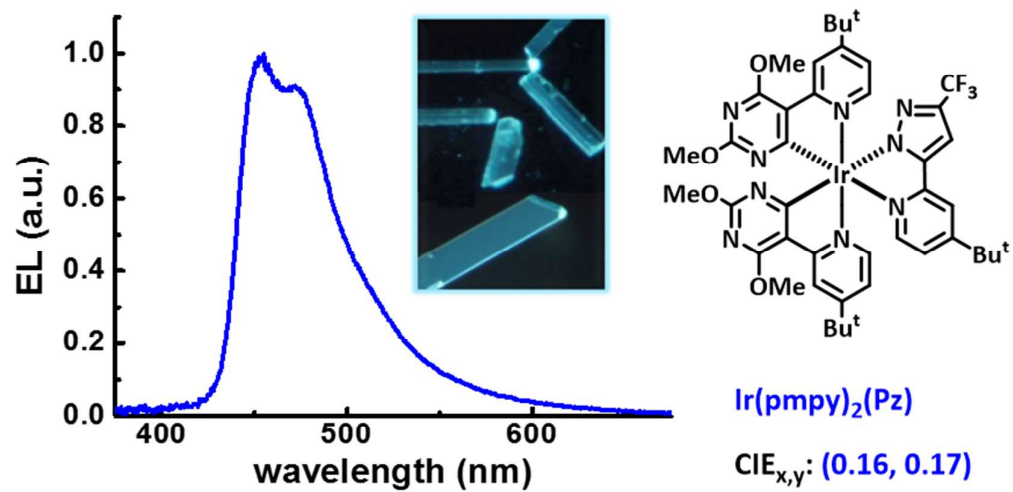
^a Turn-on voltage at which emission became detectable (10⁻² cd/m²).

1. H. Fu, Y.-M. Cheng, P.-T. Chou and Y. Chi, *Mater. Today*, 2011, **14**, 472-479.
2. P.-T. Chou, Y. Chi, M.-W. Chung and C.-C. Lin, *Coord. Chem. Rev.*, 2011, **255**, 2653-2665.
3. R. Visbal and M. C. Gimeno, *Chem. Soc. Rev.*, 2014, **43**, 3551-3574.
4. X. Yang, X. Xu and G. Zhou, *J. Mater. Chem. C*, 2015, **3**, 913-944.
5. J. V. Caspar and T. J. Meyer, *Inorg. Chem.*, 1983, **22**, 2444-2453.
6. S. Takizawa, K. Shimada, Y. Sato and S. Murata, *Inorg. Chem.*, 2014, **53**, 2983-2995.
7. Q. Sun, S. Mosquera-Vazquez, L. M. Lawson Daku, L. Guénée, H. A. Goodwin, E. Vauthey and A. Hauser, *J. Am. Chem. Soc.*, 2013, **135**, 13660-13663.
8. C.-H. Yang, Y.-M. Cheng, Y. Chi, C.-J. Hsu, F.-C. Fang, K.-T. Wong, P.-T. Chou, C.-H. Chang, M.-H. Tsai and C.-C. Wu, *Angew. Chem. Int. Ed.*, 2007, **46**, 2418-2421.
9. M. Mydlak, C. Bizzarri, D. Hartmann, W. Sarfert, G. Schmid and L. De Cola, *Adv. Funct. Mater.*, 2010, **20**, 1812-1820.
10. J.-Y. Hung, C.-H. Lin, Y. Chi, M.-W. Chung, Y.-J. Chen, G.-H. Lee, P.-T. Chou, C.-C. Chen and C.-C. Wu, *J. Mater. Chem.*, 2010, **20**, 7682-7693.
11. J. M. Fernandez-Hernandez, J. I. Beltran, V. Lemaur, M.-D. Galvez-Lopez, C.-H. Chien, F. Polo, E. Orselli, R. Froehlich, J. Cornil and L. De Cola, *Inorg. Chem.*, 2013, **52**, 1812-1824.
12. V. N. Kozhevnikov, Y. Zheng, M. Clough, H. A. Al-Attar, G. C. Griffiths, K. Abdullah, S. Raisys, V. Jankus, M. R. Bryce and A. P. Monkman, *Chem. Mater.*, 2013, **25**, 2352-2358.
13. E. Baranoff, I. Jung, R. Scopelliti, E. Solari, M. Grätzel and M. K. Nazeeruddin, *Dalton Trans.*, 2011, **40**, 6860-6867.
14. H.-J. Seo, K.-M. Yoo, M. Song, J. S. Park, S.-H. Jin, Y. I. Kim and J.-J. Kim, *Org. Electron.*, 2010, **11**, 564-572.
15. H. J. Park, J. N. Kim, H.-J. Yoo, K.-R. Wee, S. O. Kang, D. W. Cho and U. C. Yoon, *J. Org. Chem.*, 2013, **78**, 8054-8064.
16. M. Marín-Suárez, B. F. E. Curchod, I. Tavernelli, U. Rothlisberger, R. Scopelliti, I. Jung, D. Di Censo, M. Grätzel, J. F. Fernández-Sánchez, A. Fernández-Gutiérrez, M. K. Nazeeruddin and E. Baranoff, *Chem. Mater.*, 2012, **24**, 2330-2338.
17. S. Lee, S.-o. Kim, H. Shin, H.-J. Yun, K. Yang, S.-K. Kwon, J.-J. Kim and Y.-H. Kim, *J. Am. Chem. Soc.*, 2013, **135**, 14321-14328.
18. S. O. Jeon, S. E. Jang, H. S. Son and J. Y. Lee, *Adv. Mater.*, 2011, **23**, 1436-1441.
19. C. Fan, Y. Li, C. Yang, H. Wu, J. Qin and Y. Cao, *Chem. Mater.*, 2012, **24**, 4581-4587.
20. C. D. Ertl, J. Cerda, J. M. Junquera-Hernandez, A. Pertegas, H. J. Bolink, E. C. Constable, M. Neuburger, E. Orti and C. E. Housecroft, *RSC Adv.*, 2015, **5**, 42815-42827.
21. L. Chen, H. You, C. Yang, D. Ma and J. Qin, *Chem. Commun.*, 2007, 1352-1354.
22. C.-H. Yang, S.-W. Li, Y. Chi, Y.-M. Cheng, Y.-S. Yeh, P.-T. Chou, G.-H. Lee, C.-H.

- Wang and C.-F. Shu, *Inorg. Chem.*, 2005, **44**, 7770-7780.
23. F. Zhang, D. Ma, L. Duan, J. Qiao, G. Dong, L. Wang and Y. Qiu, *Inorg. Chem.*, 2014, **53**, 6596-6606.
 24. S. J. Lee, K.-M. Park, K. Yang and Y. Kang, *Inorg. Chem.*, 2009, **48**, 1030-1037.
 25. H. Oh, K.-M. Park, H. Hwang, S. Oh, J. H. Lee, J.-S. Lu, S. Wang and Y. Kang, *Organometallics*, 2013, **32**, 6427-6436.
 26. J. Frey, B. F. E. Curchod, R. Scopelliti, I. Tavernelli, U. Rothlisberger, M. K. Nazeeruddin and E. Baranoff, *Dalton Trans.*, 2014, **43**, 5667-5679.
 27. S.-C. Lo, C. P. Shipley, R. N. Bera, R. E. Harding, A. R. Cowley, P. L. Burn and I. D. W. Samuel, *Chem. Mater.*, 2006, **18**, 5119-5129.
 28. B. Beyer, C. Ulbricht, D. Escudero, C. Friebe, A. Winter, L. Gonzalez and U. S. Schubert, *Organometallics*, 2009, **28**, 5478-5488.
 29. T. Sajoto, P. I. Djurovich, A. Tamayo, M. Yousufuddin, R. Bau, M. E. Thompson, R. J. Holmes and S. R. Forrest, *Inorg. Chem.*, 2005, **44**, 7992-8003.
 30. C.-F. Chang, Y.-M. Cheng, Y. Chi, Y.-C. Chiu, C.-C. Lin, G.-H. Lee, P.-T. Chou, C.-C. Chen, C.-H. Chang and C.-C. Wu, *Angew. Chem. Int. Ed.*, 2008, **47**, 4542-4545.
 31. H. Sasabe, J.-i. Takamatsu, T. Motoyama, S. Watanabe, G. Wagenblast, N. Langer, O. Molt, E. Fuchs, C. Lennartz and J. Kido, *Adv. Mater.*, 2010, **22**, 5003-5007.
 32. S. Evariste, M. Sandroni, T. W. Rees, C. Roldan-Carmona, L. Gil-Escrig, H. J. Bolink, E. Baranoff and E. Zysman-Colman, *J. Mater. Chem. C*, 2014, **2**, 5793-5804.
 33. A. Batagin-Neto, A. P. Assis, J. F. Lima, C. J. Magon, L. Yan, M. Shao, B. Hu and C. F. O. Graeff, *J. Phys. Chem. A*, 2014, **118**, 3717-3725.
 34. J. Lee, H. Oh, J. Kim, K.-M. Park, K. S. Yook, J. Y. Lee and Y. Kang, *J. Mater. Chem. C*, 2014, **2**, 6040-6047.
 35. Y. Chi, B. Tong and P.-T. Chou, *Coord. Chem. Rev.*, 2014, **281**, 1-25.
 36. P.-I. Shih, C.-H. Chien, C.-Y. Chuang, C.-F. Shu, C.-H. Yang, J.-H. Chen and Y. Chi, *J. Mater. Chem.*, 2007, **17**, 1692-1698.
 37. P.-T. Chou, W.-S. Yu, Y.-M. Cheng, S.-C. Pu, Y.-C. Yu, Y.-C. Lin, C.-H. Huang and C.-T. Chen, *J. Phys. Chem. A*, 2004, **108**, 6487-6498.
 38. G. M. Sheldrick, *Acta Crystallogr., Sect. A.*, 2008, **64**, 112-122.
 39. M. J. Frisch, G. W. Trucks, H. B. Schlegel, G. E. Scuseria, M. A. Robb, J. R. Cheeseman, G. Scalmani, V. Barone, B. Mennucci, G. A. Petersson, H. Nakatsuji, M. Caricato, X. Li, H. P. Hratchian, A. F. Izmaylov, J. Bloino, G. Zheng, J. L. Sonnenberg, M. Hada, M. Ehara, K. Toyota, R. Fukuda, J. Hasegawa, M. Ishida, T. Nakajima, Y. Honda, O. Kitao, H. Nakai, T. Vreven, J. A. Montgomery, J. E. Peralta, F. Ogliaro, M. Bearpark, J. J. Heyd, E. Brothers, K. N. Kudin, V. N. Staroverov, R. Kobayashi, J. Normand, K. Raghavachari, A. Rendell, J. C. Burant, S. S. Iyengar, J. Tomasi, M. Cossi, N. Rega, J. M. Millam, M. Klene, J. E. Knox, J. B. Cross, V. Bakken, C. Adamo, J. Jaramillo, R. Gomperts, R. E. Stratmann, O. Yazyev, A. J. Austin, R. Cammi, C. Pomelli, J. W. Ochterski, R. L. Martin, K. Morokuma, V. G. Zakrzewski, G. A. Voth, P. Salvador, J. J. Dannenberg, S.

- Dapprich, A. D. Daniels, Farkas, J. B. Foresman, J. V. Ortiz, J. Cioslowski and D. J. Fox, *Gaussian 09, Revision D.01; Gaussian Inc.*, 2009, Wallingford, CT.
40. A. D. Becke, *J. Chem. Phys.*, 1993, **98**, 5648-5652.
 41. C. Lee, W. Yang and R. G. Parr, *Phys. Rev. B*, 1988, **37**, 785-789.
 42. V. Barone, M. Cossi and J. Tomasi, *J. Chem. Phys.*, 1997, **107**, 3210-3221.
 43. M. Cossi, G. Scalmani, N. Rega and V. Barone, *J. Chem. Phys.*, 2002, **117**, 43-54.
 44. D. Andrae, U. Häussermann, M. Dolg, H. Stoll and H. Preuss, *Theor. Chim. Acta*, 1990, **77**, 123-141.
 45. L. E. Polander, A. Yella, B. F. E. Curchod, A. N. Ashari, J. Teuscher, R. Scopelliti, P. Gao, S. Mathew, J.-E. Moser, I. Tavernelli, U. Rothlisberger, M. Gratzel, M. K. Nazeeruddin and J. Frey, *Angew. Chem. Int. Ed.*, 2013, **52**, 8731-8735.
 46. T. Noël and A. J. Musacchio, *Org. Lett.*, 2011, **13**, 5180-5183.
 47. S. Ladouceur, D. Fortin and E. Zysman-Colman, *Inorg. Chem.*, 2011, **50**, 11514-11526.
 48. V. K. Rai, M. Nishiura, M. Takimoto and Z. Hou, *J. Mater. Chem. C*, 2013, **1**, 677-689.
 49. M. Zhu and C. Yang, *Chem. Soc. Rev.*, 2013, **42**, 4963-4976.
 50. E. D. Baranoff and B. Curchod, *Dalton Trans.*, 2015, **44**, 8318-8329.
 51. C.-H. Yang, M. Mauro, F. Polo, S. Watanabe, I. Muenster, R. Fröhlich and L. De Cola, *Chem. Mater.*, 2012, **24**, 3684-3695.
 52. H.-Y. Li, L. Zhou, M.-Y. Teng, Q.-L. Xu, C. Lin, Y.-X. Zheng, J.-L. Zuo, H.-J. Zhang and X.-Z. You, *J. Mater. Chem. C*, 2013, **1**, 560-565.
 53. S. Stagni, S. Colella, A. Palazzi, G. Valenti, S. Zacchini, F. Paolucci, M. Marcaccio, R. Q. Albuquerque and L. De Cola, *Inorg. Chem.*, 2008, **47**, 10509-10521.
 54. F. Kessler, Y. Watanabe, H. Sasabe, H. Katagiri, M. K. Nazeeruddin, M. Grätzel and J. Kido, *J. Mater. Chem. C*, 2013, **1**, 1070-1075.
 55. J.-L. Chen, C.-H. Lin, J.-H. Chen, Y. Chi, Y.-C. Chiu, P.-T. Chou, C.-H. Lai, G.-H. Lee and A. J. Carty, *Inorg. Chem.*, 2008, **47**, 5154-5161.
 56. C.-W. Hsu, C.-C. Lin, M.-W. Chung, Y. Chi, G.-H. Lee, P.-T. Chou, C.-H. Chang and P.-Y. Chen, *J. Am. Chem. Soc.*, 2011, **133**, 12085-12099.
 57. H. Fukagawa, K. Watanabe, T. Tsuzuki and S. Tokito, *Appl. Phys. Lett.*, 2008, **93**, 133312.
 58. Y.-K. Kim, J. Won Kim and Y. Park, *Appl. Phys. Lett.*, 2009, **94**, 063305.
 59. W.-Y. Hung, L.-C. Chi, W.-J. Chen, Y.-M. Chen, S.-H. Chou and K.-T. Wong, *J. Mater. Chem.*, 2010, **20**, 10113-10119.
 60. M.-T. Kao, W.-Y. Hung, Z.-H. Tsai, H.-W. You, H.-F. Chen, Y. Chi and K.-T. Wong, *J. Mater. Chem.*, 2011, **21**, 1846-1851.
 61. W.-Y. Hung, Z.-W. Chen, H.-W. You, F.-C. Fan, H.-F. Chen and K.-T. Wong, *Org. Electron.*, 2011, **12**, 575-581.
 62. S.-J. Su, E. Gonmori, H. Sasabe and J. Kido, *Adv. Mater.*, 2008, **20**, 4189-4194.
 63. Y.-Y. Lyu, J. Kwak, W. S. Jeon, Y. Byun, H. S. Lee, D. Kim, C. Lee and K. Char, *Adv. Funct. Mater.*, 2009, **19**, 420-427.

64. S. H. Kim, J. Jang, S. J. Lee and J. Y. Lee, *Thin Solid Films*, 2008, **517**, 722-726.
65. H.-H. Chang, W.-S. Tsai, C.-P. Chang, N.-P. Chen, K.-T. Wong, W.-Y. Hung and S.-W. Chen, *Org. Electron.*, 2011, **12**, 2025-2032.
66. N. Chopra, J. Lee, Y. Zheng, S.-H. Eom, J. Xue and F. So, *Appl. Phys. Lett.*, 2008, **93**, 143307.
67. D. Tanaka, T. Takeda, T. Chiba, S. Watanabe and J. Kido, *Chem. Lett.*, 2007, **36**, 262-263.
68. C. Han, G. Xie, H. Xu, Z. Zhang, D. Yu, Y. Zhao, P. Yan, Z. Deng, Q. Li and S. Liu, *Chem. Eur. J.*, 2011, **17**, 445-449.
69. R. Srivastava and L. R. Joshi, *Phys. Chem. Chem. Phys.*, 2014, **16**, 17284-17294.
70. Y. Zhao, J. Tang, H. Zhang and Y. Ma, *Eur. J. Inorg. Chem.*, 2014, **2014**, 4843-4851.
71. Y.-H. Kim, J.-B. Kim, S.-H. Han, K. Yang, S.-K. Kwon and J.-J. Kim, *Chem. Commun.*, 2015, **51**, 58-61.
72. J.-H. Lee, G. Sarada, C.-K. Moon, W. Cho, K.-H. Kim, Y. G. Park, J. Y. Lee, S.-H. Jin and J.-J. Kim, *Adv. Opt. Mater.*, 2015, **3**, 211-220.
73. M. Cocchi, D. Virgili, V. Fattori, D. L. Rochester and J. A. G. Williams, *Adv. Funct. Mater.*, 2007, **17**, 285-289.
74. S. Reineke, G. Schwartz, K. Walzer and K. Leo, *Appl. Phys. Lett.*, 2007, **91**, 123508.



Ir(III) complexes with functional 2-(pyrimidin-5-yl)pyridine cyclometalates display blue electroluminescence and with CIE_{x,y} coordinates occurred at (0.16, 0.17) at 100 cd/m².